JOURNAL OF MATERIALS SCIENCE 20 (1985) 407–413

Precipitation of an ordered intermetallic phase in WC–10% Ni

HAYDÉE LE ROUX
Boart Basic Research Group, Physics Department, University of the Witwatersrand, Johannesburg, Republic of South Africa

The cause of the variability of the intensity of magnetization of the nickel binder phase in cemented carbides was sought by electron diffraction and dark-field microscopy studies of fractured specimens, one of which was partially magnetic and the other almost non-magnetic. A coherent phase in the nickel binder having either a b c c or a CsCl-type structure was found on the boundaries of crack paths. A coherent non-randomly arranged CsCl-type phase was found in an epitaxial relationship with (1 2 . 0) planes of WC. The lattice parameter $a = 0.295$ nm for both coherent phases. This phase or phases occurs more frequently in non-magnetic than in magnetic nickel binders of hardmetals. When seen near WC grains the ordered phase is often accompanied by randomly arranged tungsten trioxide particles. The implication is that the ordered phase occurs more readily in carbon-deficient surroundings. The phase is postulated to be NiW because large quantities of tungsten are known to form solid solutions with nickel.

1. Introduction

Although the traditional binder material in cemented carbides is cobalt (face centred cubic: lattice parameter $a = 0.354$ nm), the need for alternative binders arises from time to time and several studies of the suitability of nickel (f c c, $a = 0.352$ nm) have been made (e.g. [1]). Whereas the magnetic moment of cobalt as binder phase is practically the same as that of the pure metal, nickel as the binder phase was found to be either almost non-magnetic in half of the specimens or to have about 60% of the magnetic moment in the remaining specimens [1]. The non-magnetic state is generally believed to be due to the large quantities (~ 20%) of tungsten (body centred cubic: $a = 0.317$ nm) dissolved in nickel.

The large solubility of tungsten in nickel was first reported by Takeda [2], who also pointed out that because of this large quantity of dissolved tungsten, the nominal content of the nickel binder phase increases. For example, in WC–6 wt% Ni, the binder phase increases to ~ 9 wt% after sintering. This behaviour contrasts with that of cobalt which dissolves small quantities of tungsten, i.e. < 5%, and this dissolution is inhibited by interstitially dissolved carbon.

Recently, Fiedler and Stadelmeier [3] confirmed the presence of an extended phase field of tungsten in WC–Ni. The formation of various ternary carbides was reported for the 50–50 Ni–W compositional range. The solubility of tungsten and carbon in nickel is, according to Chaporova *et al.* [4], independent of tungsten and carbon content. According to the same authors, the solid solubility limit of WC in nickel, in the presence of free carbon, is ~ 15 wt%.

The exact dependence of the magnetization on the amount of tungsten dissolved in cobalt was determined by Tillwick and Joffe [5]. A similar relationship between magnetization and amount of tungsten dissolved in nickel is not known. As shown in the Ni–W phase diagram [6] the Curie temperature of nickel decreases from 300° C to below room temperature by the dissolution of about 6 at% tungsten (~ 15 wt%). Nickel in cemented carbides containing this quantity of tungsten will, therefore, be paramagnetic. If considerably less than 15 wt% tungsten should be dissolved then the nickel can be expected to be partially magnetic. Any decrease in magnetization may be caused either by the concentration of whatever tungsten is present in

0022–2461/85 $03.00 + .12

particular regions, thus reducing the Curie temperature in those regions, or by a decrease in the magnetic moment. The reported solubilities of tungsten in nickel would be sufficient to bring about a non-magnetic state.

An intermetallic compound WNi_4 (tetragonal, $a = 0.573$ nm, $c = 0.355$ nm) is said to form peritectoidally in the Ni–W system at $\sim 900^\circ$ C at a tungsten composition of about 40 wt% [6]. The existence of binary intermetallic compounds in the WC–Ni system has not yet been reported.

Only elements with the same crystal structure, where atom sizes differ by less than 15%, can form continuous solid solutions. If unlike atoms attract each other in solid solutions, then superlattices may form [7]. Local strains caused by the irregular distribution of atoms of different size in solid solution can be lessened on ordering into superlattices. Nickel is known to form ordered superlattice CsCl-type structures with gold and aluminium, both of which are f c c, with zinc (h c p) and titanium (h c p or b c c) [6]. The difference in atomic size between nickel and titanium is greater than between nickel and gold or between nickel and aluminium, which are, in turn, greater than between nickel and zinc. The difference between nickel and tungsten atoms which do not form continuous solid solutions is about 11% and is almost the same as for nickel and zinc. The lattice parameters of NiZn and NiTi are, respectively, 0.29 and 0.30 nm, [6].

Evidence for the existence of an ordered, CsCl-type, intermetallic compound is presented in this paper.

2. Experimental details

Electron diffraction and dark-field electron microscopy studies were carried out on a Jeol 100C transmission electron microscope to observe the structures of the phases and their interrelationships. The smallest diffraction aperture of 1 μm diameter was used. The standards used were the known phases contained in the material.

2.1. Specimens

The specimens examined were those that had been fractured by Brabyn *et al.* [1]. The magnetic moment of pure nickel is 62 $(\mathrm{T\,m^3\,kg^{-1}}) \times 10^{-7}$. The magnetic specimen (E1) had a magnetization of about 46 units and the non-magnetic specimen (E2) about 1.5 units. Mechanical properties for E2 were not reported by Brabyn *et al.*, as non-magnetic specimens were usually rejects.

2.2. Thin specimen preparation

Rectangular plates ~ 0.2 mm thick and 0.5 cm x 1 cm in cross-section were sliced from the fractured material near the fracture edge, using a diamond saw. The parallel-sided plates obtained were thinned by electrolytic etching to a thickness of ~ 50 μm after which the samples were thinned to transparency by ion-beam milling. Specimen E1 was 0.86 mm and specimen E2 was 5.6 mm distant from the fracture edge.

3. Results and discussion

An intensive investigation of both the binder phase and WC (hexagonal: $a = 0.291$, $c = 0.284$ nm) grains revealed that a wide-spread ordering reaction took place in the non-magnetic specimens. The same reaction occurred in the magnetic material though to a lesser extent.

The (1 1 1) plane of a b c c (disordered) or CsCl-type (superlattice) structure was observed in 40% of the non-magnetic nickel lakes and in 18% of magnetic nickel lakes examined. The (1 0 0) plane of a superlattice structure was seen in an epitaxial relationship mainly with (1 2 .0) planes of WC grains. The orientation relationship is as follows:

$$(1\,2\,.\,0)\ \mathrm{WC} \parallel (1\,0\,0)\ \text{superlattice}$$

$$[2\,\bar{1}\,.\,0]\ \mathrm{WC} \parallel [0\,\bar{1}\,0]\ \text{superlattice}$$

$$[0\,0\,.\,1]\ \mathrm{WC} \parallel [0\,0\,1]\ \text{superlattice.}$$

The lattice parameter of the ordered phase is 0.295 nm and is 7% smaller than the lattice parameter of tungsten. The ordered phase cannot be tungsten nor can it be any of the ternary carbides which are all large-grained.

The morphology of the ordered phase is illustrated in conventional dark-field micrographs in Figs. 1b and c where the phase is next to a nickel lake and in Figs. 3b and c where it is shown in relation to a WC grain. The respective selected-area diffraction patterns (SADPs) are given in Figs. 1a and 3a.

In Fig. 1a the strong reflections, numbered 1 to 4, lie in the [2 3 3] zone of f c c nickel. The inner, weaker, reflections are 1 1 0-type superlattice reflections lying on the [1 1 1] b c c or CsCl-type zone. The SADP is correctly oriented with respect to the images. The ordered phase is

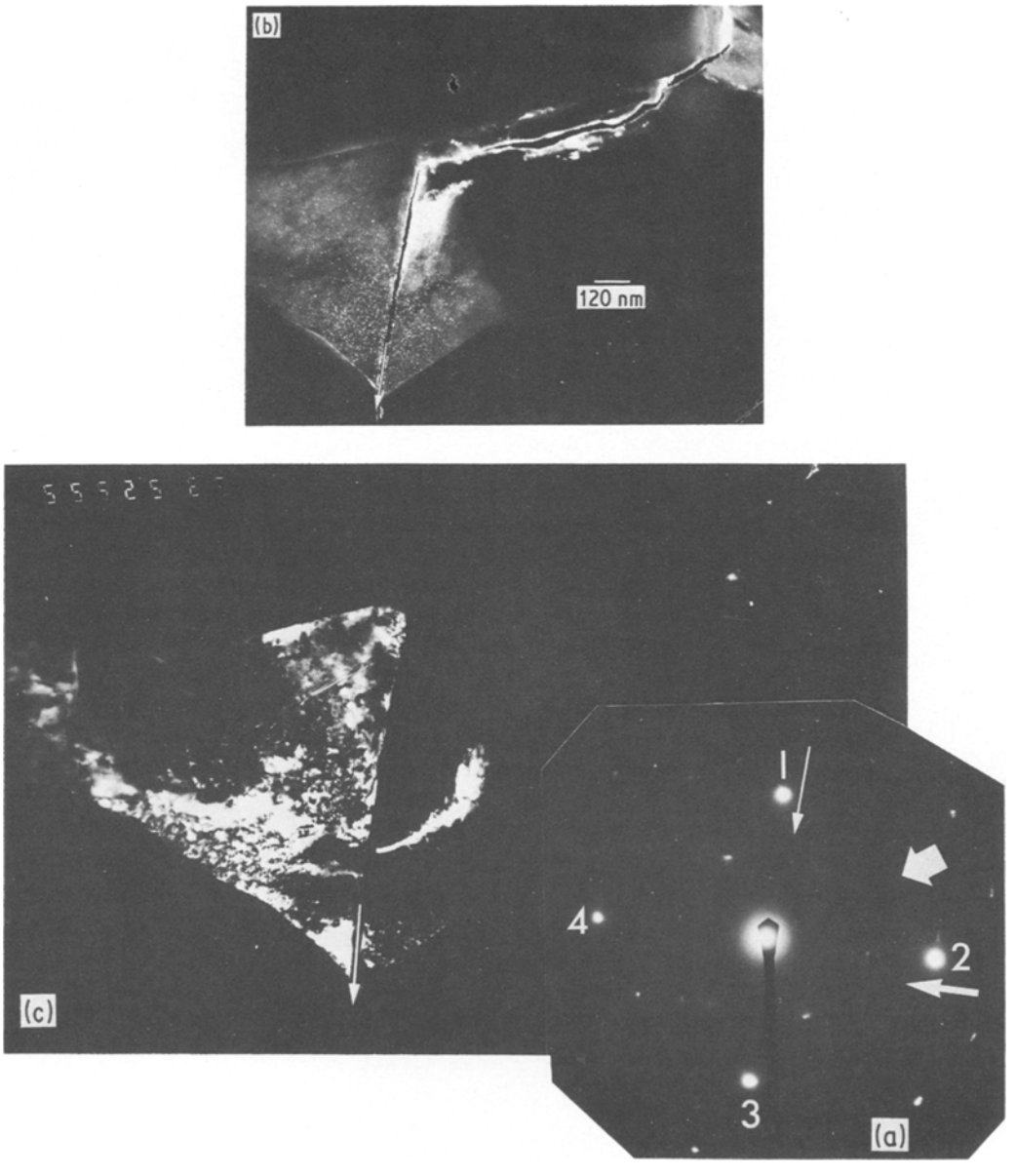

Figure 1 (a) SADP of a nickel lake. This SADP has been corrected for rotation with respect to the images. Strong spots numbered 1 to 4 are 0 2 2 and 3 1 1 type reflections in the [2 3 3] f c c zone. The thin arrow points in the $[0\,1\,\bar{1}]$ direction. The inner weak spots are 1 1 0 type reflections in the [1 1 1] b c c/superlattice zone. The nickel and the superlattice are in an exact orientation relation. The (2 3 3) f c c plane is parallel to the (1 1 1) superlattice plane. $[0\,1\,\bar{1}]$ f c c ($\parallel [1\,1\,\bar{2}]$ superlattice) is marked with a thin arrow at spot 1 which is a combined $0\,\bar{2}\,2$ f c c and $\bar{1}\,\bar{1}\,2$ superlattice reflection. At spot 2 ($3\,\bar{1}\,\bar{1}$ f c c and $2\,\bar{2}\,0$ superlattice reflections) a medium thick arrow points in the $[\bar{3}\,1\,1]$ f c c $\parallel [\bar{1}\,1\,0]$ superlattice direction. The short thick arrow indicates the $[\bar{1}\,2\,\bar{1}]$ b c c/superlattice direction. (b) Composite conventional dark-field micrograph obtained by the superposition of three images obtained from three different weak 1 1 0 b c c/superlattice-type, ($\bar{1}\,1\,0$, $\bar{1}\,0\,1$ and $0\,\bar{1}\,1$) reflections. The crack passes through the ordered phase along $[\bar{1}\,2\,\bar{1}]$ and then along $[1\,1\,\bar{2}] \parallel [0\,1\,\bar{1}]$ f c c (thin arrow). The spotted shadowy region is the [2 3 3] zone of an f c c nickel lake shown separately in Fig. 1c. (c) Dark-field micrograph imaged with spot 3 which is a combined strong $0\,2\,\bar{2}$ nickel and weak $1\,1\,\bar{2}$ superlattice reflection. The thin arrow points in the $[0\,1\,\bar{1}]$ f c c direction.

coherent with the nickel lattice, the orientation relationship being:

$[0\,1\,\bar{1}]$ f c c$\|[1\,1\,\bar{2}]$ b c c/superlattice

(thin arrow)

$[\bar{3}\,1\,1]$ f c c$\|[\bar{1}\,1\,0]$ b c c/superlattice

(medium thick arrow)

$(2\,3\,3)$ f c c$\|(1\,1\,1)$ b c c/superlattice.

A series of dark-field micrographs imaged separately with spots selected from both the strong and weak pattern in Fig. 1a was obtained. A composite dark-field micrograph, Fig. 1b, was made by the superposition of images of three different weak inner spots, ($\bar{1}\,1\,0$, $\bar{1}\,0\,1$ and $0\,\bar{1}\,1$), in the SADP in 1a. This region lies on the boundary of the nickel lake, shown in Fig. 1c, as imaged with spot 3, a combined strong $0\,2\,\bar{2}$ nickel and weak $1\,1\,\bar{2}$ superlattice reflection. After changing direction the crack propagates through the nickel lake along the $[0\,1\,\bar{1}]$ f c c crystallographic direction (thin arrow). The corresponding crack path through the ordered phase is along the $[1\,1\,\bar{2}]$ direction (thin arrow) having changed from $[\bar{1}\,2\,\bar{1}]$ (short thick arrow). The direction of propagation is arbitrary. It could be in the reverse direction without altering any conclusions.

The more usual orientation relationship observed between nickel and the superlattice, not illustrated in dark field, is shown in the SADP in Fig. 2:

$[1\,\bar{1}\,\bar{1}]$ f c c$\|[\bar{1}\,1\,0]$ b c c/superlattice

(thin arrow)

$[0\,1\,\bar{1}]$ f c c$\|[1\,1\,\bar{2}]$ b c c/superlattice

(thick arrow)

$(2\,1\,1)$ f c c$\|(1\,1\,1)$ b c c/superlattice

The SADP in Fig. 3a should be rotated anticlockwise through an angle of about 30° to bring it into coincidence with the images. The thin arrows in Figs. 3a and b will then be parallel.

Fig. 3b is the dark-field image of spot 1 shown in Fig. 3a. An identical image was obtained with spot 5. Dark-field images having fringes in the same positions as in Fig. 3b were also obtained separately with spots 2, 3, 4, 6, 7 and 8 but are not illustrated. The reflections 1 to 8 all lie in the $(1\,2\,.\,0)$ plane of WC.

Fig. 3c is the dark-field image of one of the

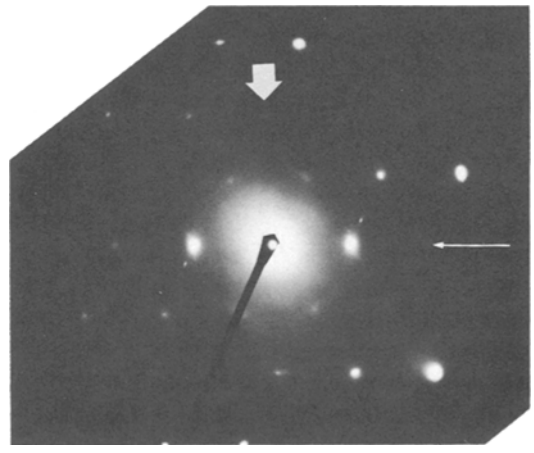

Figure 2 SADP of the $(2\,1\,1)$ plane of a nickel lake in an orientation relation with the $(1\,1\,1)$ plane of the ordered phase. The thick arrow indicates the $[0\,1\,\bar{1}]$ f c c parallel to the $[1\,1\,\bar{2}]$ b c c/superlattice direction. The thin arrow indicates the $[1\,\bar{1}\,\bar{1}]$ f c c is parallel to $[\bar{1}\,1\,0]$ b c c/superlattice direction. The f c c $(2\,1\,1)$ plane is parallel to the $(1\,1\,1)$ b c c/superlattice plane. No dark-field micrographs are shown.

elongated spots marked with small vertical arrows and shows non-randomly arranged clusters of acicular particles which are coherent with the WC matrix. Only one dark-field image is illustrated as all are similar. These diffraction spots are the $1\,1\,0$ type reflections of a $(1\,0\,0)$ plane of a superlattice. The $0\,0\,1$-type reflections are nearly coincident with the WC spots at 1 and 5 which are $0\,0\,.\,1$-type reflections. There is a small difference between the lattice parameters and, hence, a small misfit between the reflections in the two planes. The second order $0\,0\,2$ superlattice reflection, marked with a small horizontal arrow, is sufficiently separated from the $0\,0\,.\,2$ WC reflection to be visible. The axes of the particles are aligned along the $[0\,0\,.\,1]$ WC direction (thin arrows in Fig. 3a and b) and these axes are normal to the elongation of the particle reflections. All dark-field images of WC reflections have thickness fringes. By comparing the positions of the fringes with the clusters of coherent particles a one-to-one correspondence is apparent. The fringes are therefore interpreted to be interfacial fringes which can be imaged either by strong matrix or by strong particle reflections [8]. The orientation relation between the two crystals is described in paragraph 2 of this section.

Fig. 4a was imaged with an arc of the diffuse ring marked "R" in the SADP in Fig. 3a. This ring

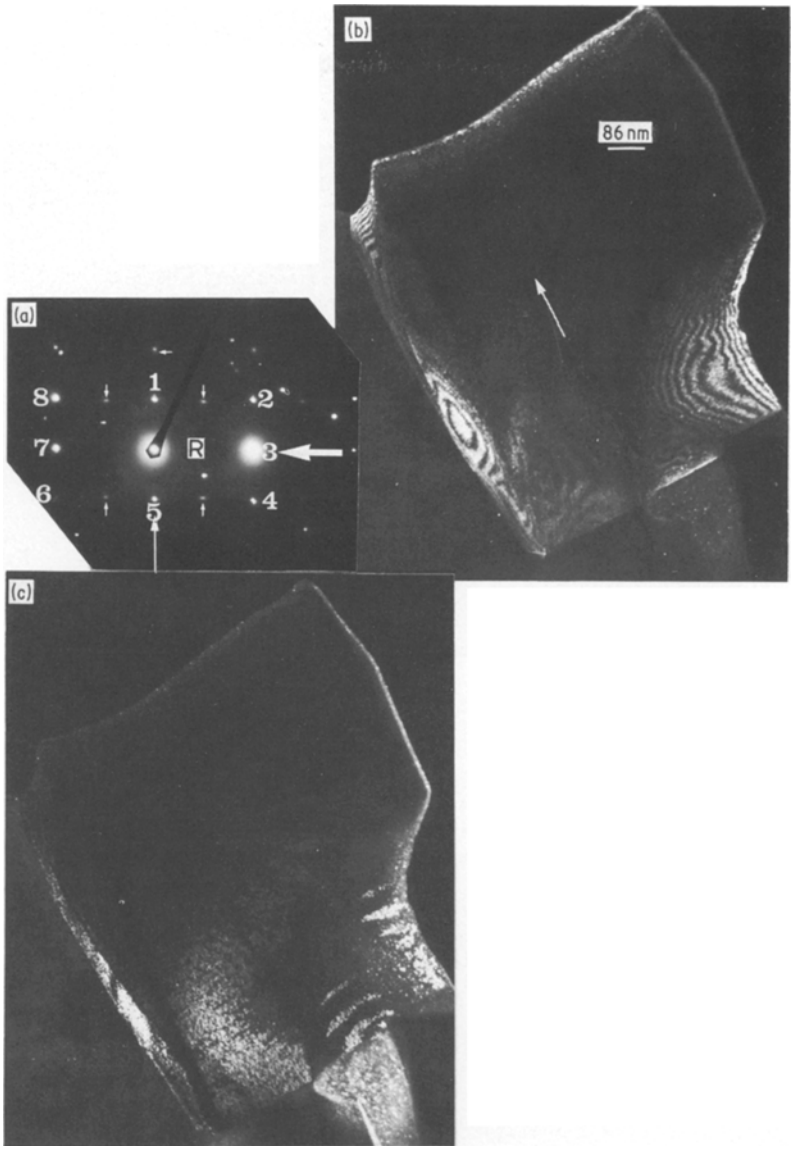

Figure 3 (a) SADP of the WC grain in Fig. 3b. This pattern should be rotated anticlockwise through ~ 30° so that the thin arrows in (a) and (b) are parallel. Spots numbered 1 to 8 are WC reflections lying in the (1 $\bar{2}$. 0) plane. Spots marked with small vertical arrows are 1 1 0 type reflections of a superlattice lying in a (1 0 0) plane. These two planes are parallel and there is an orientation relation between the two phases. The [0 0 . 1] hexagonal direction (thin arrow) is parallel to the [0 0 1] superlattice direction and the [2 $\bar{1}$. 0] hexagonal direction (short arrow) is parallel to the [0 $\bar{1}$ 0] superlattice direction. The 0 0 1 type superlattice reflections are not quite coincident with 0 0 . 1 WC reflections at spots 1 and 5, as there is a small misfit between the two planes due to a difference in the lattice parameters of the two phases. The small horizontal arrow indicates an 0 0 2 superlattice reflection which is sufficiently separated from the 0 0 . 2 WC reflection to be visible. The diffuse ring marked "R" is described in Fig. 4. (b) Dark-field micrograph imaged with spot 1. Thickness fringes are visible, The image of spot 5 is the same as that of spot 1 and is not shown. Separate dark-field images of spots 2, 3, 4, 6, 7 and 8 (also not shown) all have fringes in the same positions as in (b). All these spots are slightly displaced from the spots in the (1 0 0) plane of the superlattice due to the lattice misfit, (WC: $a = 0.251$ nm, $c = 0.283$ nm; superlattice: $a = 0.295$ nm). (c) Dark-field micrograph imaged by one of the elongated superlattice reflections marked with small vertical arrows. Only one of the images is illustrated as all are similar. Fine, acicular particles non-randomly arranged with their long axes aligned along the [0 0 . 1] hexagonal direction are coherent with the WC matrix. The particle axes also lie normal to the elongation of their reflections. The thickness fringes seen in (b), imaged with strong matrix reflections, are in a one-to-one correspondence with the positions of the coherent particles in (c) and are believed to be interfacial fringes which can be imaged with either strong matrix or strong particle reflections [8].

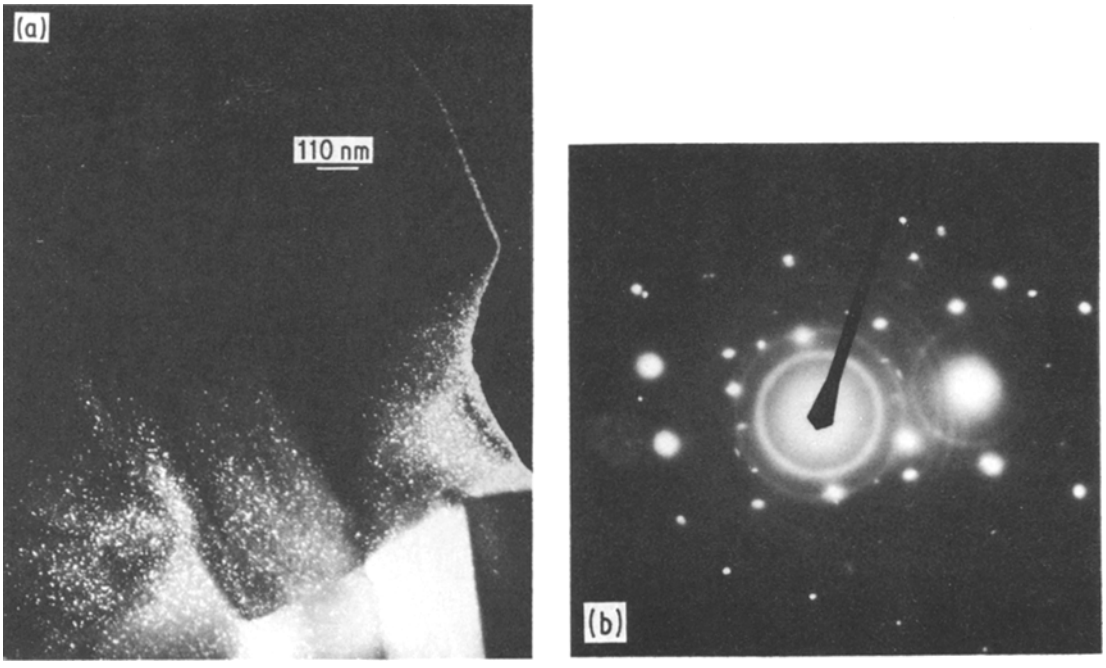

Figure 4 (a) Dark-field micrograph imaged with an arc of the diffuse ring in Fig. 3a (marked "R") with d-value = ~ 0.38 nm. These particles are randomly arranged, in contrast to the neighbouring coherent ordered phase. (b) SADP of the WC grain, shown in Fig. 3, taken after several exposures of the grain to the electron beam had been made. It is assumed that the particles were heated up in the electron beam ([8], p. 59). This set of rings, which appeared suddenly, was found to have d-values of 0.376, 0.270, 0.186, 0.166, and 0.153 nm. These d-values match those of the high-temperature form (770° C) of tungsten trioxide [9]. The low temperature form of tungsten trioxide has d-values of 0.384, 0.376, 0.364 (each of 100% intensity), 0.268, 0.266, 0.262, 0.182 and 0.164 nm ([9], p. 84). The mean d-value of the first three rings is 0.381 nm. This is the only ring that can be seen in Fig. 3a. The diffuseness of this and other rings (which are not visible in the print), of the low-temperature form, compared to the sharpness of the rings of the high-temperature form in this figure, suggest that the particles are less well crystallized before than after the heat-treatment.

has a d-value of ~ 0.38 nm. The dark-field image shows randomly arranged particles in the neighbourhood of the coherent ordered phase. After repeated viewings of the area in Fig. 4a the appearance of the ring "R" changed from diffuse to sharp and several additional rings became visible, as shown in Fig. 4b. On indexing these sharp rings they were found to have d-values of 0.376, 0.270, 0.186, 0.166 and 0.153 nm which correspond to those of the *high temperature* (770° C) form of tungsten trioxide (cf. [9], p. 98). The diffuseness of the original rings of which only the strongest is visible in Fig. 3a and which are believed to be those of the *low temperature* form of tungsten trioxide, suggest that the state of crystallization of these particles is poor. The d-values of this low temperature form ([9], p. 84) are 0.384, 0.376, 0.364, 0.268, 0.266, 0.262, 0.182 and 0.164 nm and the intensity of each of the first three rings is 100%. Carbides are poor thermal conductors and heat up easily in the electron beam ([8], p. 59).

It has been concluded, from the presence of tungsten trioxide in the neighbourhood of the ordered phase, that the material is carbon deficient in this region.

4. Conclusions

The most probable composition of the unknown phase is nickel and tungsten in equal proportions which, in the fully ordered state, would have one of the elements occupying positions at the corners of the unit crystal cell and the other the body centred position. The disordered b c c phase has equal probabilities of the different atoms occupying either position. There is no evidence that the (1 1 1) b c c pattern observed is not that of the CsCl-type (1 1 1) plane. The observed lattice parameter is similar to those of NiTi and NiZn.

The suggested composition is in keeping with high solubilities of tungsten in nickel.

The presence of tungsten trioxide in the neighbourhood of ordered NiW confirms that there are localized regions which are deficient in carbon. Since more of the ordered phase has been seen in non-magnetic than in magnetic material and since 60% of the magnetization could be retained in this material during manufacture it is concluded that an adequate quantity of carbon is necessary to control the dissolution of W. The control of carbon content is a critical procedure even in carbides cemented with Co.

The evidence of the crack propagation through the ordered phase implies that this phase is an embrittling medium.

Acknowledgements

The author wishes to thank Mrs S. S. Taylor for excellent technical assistance, Dr C. Peters of the Boart Research Centre, for specimens and discussions, and the sponsors, Boart Research Centre, Krugersdorp for generous financial support.

References

1. S. M. BRABYN, R. COOPER and C. T. PETERS, Proceedings 10th Plansee Seminar, Tyrol, Austria, Vol. 2 (Metallwerk Plansee GmbH, Reutte, Austria, 1981) p. 675.
2. S. TAKEDA, *Sci. Rep. Tohoku Imperial Univ. Honda Anniv. Issue* (1936) 864.
3. MARIA-LUISE FIEDLER and H. H. STADELMAIER, *Z. Metallkde* **66** (1975) 403.
4. I. N. CHAPOROVA, V. I. TRET'YAKOV, E. A. SHCHETILINA and T. G. MAKARENKO, *Tvedye Splavy Sbovnik Trudov Vsesoyuz. Nauch. Issledovat. Inst. Tverd. Splavov* **1** (1959) 177.
5. D. L. TILLWICK and I. JOFFE, *Scripta Metall.* 7 (1973) 479.
6. M. HANSEN and K. ANDERKO, "Constitution of Binary Alloys" (McGraw-Hill, New York, 1958) pp. 1049, 1059.
7. C. S. BARRETT, "Structure of Metals" (McGraw-Hill, London 1953) p. 221.
8. P. B. HIRSCH, A. HOWIE, R. B. NICHOLSON, D. W. PASHLEY and M. J. WHELAN, "Electron Microscopy of Thin Crystals" (Butterworths, London, 1965) p.346.
9. "Inorganic Index to the Powder Diffraction File", ASTM Publications PD 1S-171 (American Society for Testing and Materials, Philadelphia, 1967) p. 98.

Received 20 December 1983
and accepted 13 March 1984